Click Here
for
Full Article

Nonmigrating semidiurnal tide over the Arctic determined from TIMED Doppler Interferometer wind observations

H. Iimura,[1] D. C. Fritts,[1] Q. Wu,[2] W. R. Skinner,[3] and S. E. Palo[4]

[1]   The TIMED Doppler Interferometer (TIDI) on the NASA Thermosphere Ionosphere Mesosphere Energetics and Dynamics (TIMED) satellite has been measuring horizontal winds in the mesosphere and lower thermosphere (MLT) since 2002. Because of the high inclination of the TIMED orbit, TIDI measures the horizontal winds from pole to pole every orbit. This paper presents the first assessment of the spatial structure and temporal evolution of the nonmigrating semidiurnal tides over the Arctic determined from the TIDI wind measurements and a comparison of the structure of the nonmigrating semidiurnal tide between the Arctic and Antarctic. The nonmigrating semidiurnal tides were determined as a 60 day average based on the yaw cycles of the spacecraft. The nonmigrating semidiurnal tidal wind field over the Arctic comprises mainly the westward-propagating zonal wave numbers 1 (W1) and 3 (W3) and standing zonal wave number 0 (S0) modes. The W1 mode is the most prominent, maximizing above 90 km poleward of 60°N during the yaw interval ranging from mid-March to mid-May. While this mode exhibits a slight amplitude increase toward the North Pole during this interval, its phase is nearly constant with latitude. The S0 mode is enhanced over two yaw intervals ranging from mid-January to mid-May, but its amplitude decreases toward the North Pole. Compared to the W1 semidiurnal tide over the Antarctic, that over the Arctic is smaller in amplitude, of less extended duration, achieves maximum amplitudes at higher altitudes by ~10 km, and exhibits a weaker amplitude increase toward the pole. These differences likely result from differences in excitation mechanisms and efficiency and/or in propagation conditions in the two responses for the nonmigrating semidiurnal tides between the Arctic and Antarctic.

1. Introduction

[2]   Atmospheric tides are one of the most prominent features of the wind field in the mesosphere and lower thermosphere (MLT). These arise primarily from solar thermal absorption in the troposphere and lower stratosphere, grow in amplitude as they propagate to higher altitudes, and attain local amplitudes as high as ~50 to 100 ms^{-1} or greater extending from the MLT to much higher altitudes [*Kato*, 1980; *Lindzen*, 1990]. The solar tidal periods are harmonics of a solar day and they comprise both migrating (Sun-synchronous) and nonmigrating modes due to longitudinal variations in the linear and nonlinear sources [*Hagan and Forbes*, 2002, 2003].

[3]   Global tidal structure in an idealized atmosphere, including all the various modes, can be described by Laplace's tidal equation and represented as a superposition of an infinite series of eigenfunctions, referred to as Hough functions [*Chapman and Lindzen*, 1970; *Volland*, 1988]. Hough functions, or Hough modes, are characterized by two indices (s, n), where s and n are related to the longitudinal and latitudinal structure and used to indicate the zonal wave number and meridional index. The Hough functions indicate that the dominant contributions to the tidal field at low latitudes are the first symmetric migrating modes, for example the $(1, 1)$ mode for the diurnal tide and the $(2, 2)$ mode for the semidiurnal tide [*McLandress et al.*, 1996]. These Hough functions are expanded for the tidal wind field, as Hough Function Expansions (HFEs) [*Chapman and Lindzen*, 1970; *Forbes*, 1982a, 1982b, 1995]. On the basis of the HFEs, the diurnal $(1, 1)$ mode maximizes equatorward of ~30° while the semidiurnal $(2, 2)$ mode maximizes at latitudes of ~55°.

[1]Colorado Research Associates Division, NorthWest Research Associates Inc., Boulder, Colorado, USA.
[2]High Latitude Observatory, National Center for Atmospheric Research, Boulder, Colorado, USA.
[3]Space Physics Research Laboratory, University of Michigan, Ann Arbor, Michigan, USA.
[4]Department of Aerospace Engineering Sciences, University of Colorado at Boulder, Boulder, Colorado, USA.
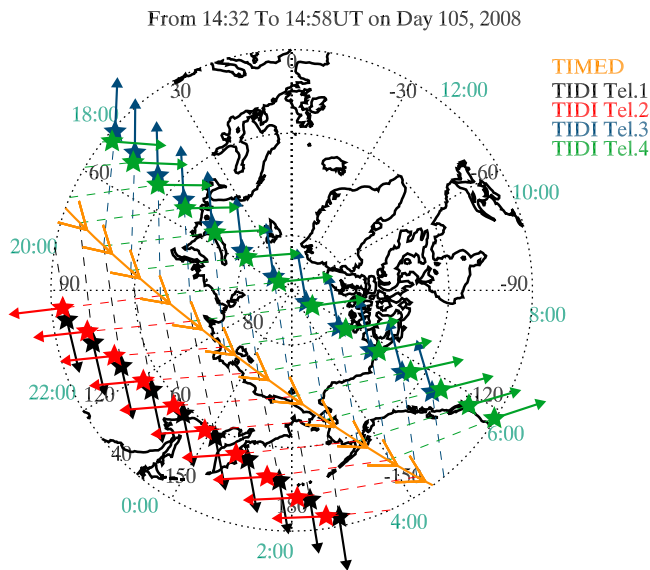
From 14:32 To 14:58UT on Day 105, 2008

Figure 1. Ground track of the TIMED spacecraft (yellow arrows) and locations of TIDI measurements poleward of 40°N from 1432 to 1458 UT on day 105, 2008. Measurement locations of the four TIDI telescopes are shown by black (telescope 1), red (telescope 2), blue (telescope 3), and green (telescope 4) stars. Arrows from the TIDI measurement locations show the viewing directions of the telescopes. Local time is indicated on the circumference of the figure.

[4] In the HFE theory, amplitudes of tides a with a zonal wave number s are expected to vary as $a \sim \sin^{s-1}\theta$ [*Forbes et al.*, 1999a], where θ is colatitude. Hence the HFEs predict that amplitudes of the tides with s ($\neq 1$) decrease with latitude toward the pole. On the other hand, amplitudes of tides with $s = 1$ are expected to remain constant poleward of ~60°. Therefore, the tidal field in the vicinity of the poles is expected to comprise primarily the $s = 1$ mode.

[5] These theoretical predictions for the semidiurnal tide at high latitudes were first verified by *Hernandez et al.* [1993] from OH airglow emission wind measurements at South Pole during winter. Seasonal variations of the westward-propagating zonal wave number 1 (W1) semidiurnal tide in the vicinity of the South Pole were subsequently observed by a meteor radar [*Forbes et al.*, 1995]. These observations revealed that the W1 mode was enhanced during summer [*Portnyagin et al.*, 1998; *Forbes et al.*, 1995, 1999b; *Lau et al.*, 2006]. *Portnyagin et al.* [1998] compared the W1 mode determined from South Pole measurements with the measurements at lower latitudes in Antarctica and concluded that the W1 mode dominated poleward of ~75°S. Recent analyses from radar measurements at multiple stations on the coast of Antarctica by *Murphy et al.* [2006] determined that the semidiurnal tidal wind field is a mixture of the W1, westward-propagating zonal wave numbers 2 and 3 (W2 and W3), and the standing zonal wave number 0 (S0) modes.

[6] Ground-based wind measurements have also been made at various locations in the Arctic [*Hocking*, 2001; *Fisher et al.*, 2002; *Kishore et al.*, 2002; *Mitchell et al.*, 2002; *Aso*, 2003; *Wu et al.*, 2003; *Merzlyakov et al.*, 2005; *Nozawa et al.*, 2005; *Singer et al.*, 2005; *Hoffmann*

et al., 2007], and tidal structures over the Arctic and Antarctic have been compared employing these measurements [*Avery et al.*, 1989; *Portnyagin et al.*, 1993; *Fraser et al.*, 1995; *Riggin et al.*, 2003]. However, it has proven impossible to determine unambiguously the tidal modes from the limited ground-based measurements in the Arctic and Antarctic. As a result, the structures of the tidal modes predicted by models in the high-latitude MLT [*Angelats i Coll and Forbes*, 2002; *Mayr et al.*, 2005; *Miyahara and Miyoshi*, 1997; *Yamashita et al.*, 2002] have not been compared with measurements [*Du et al.*, 2007].

[7] A number of studies have employed wind measurements by the TIMED Doppler Interferometer (TIDI) on board the Thermosphere Ionosphere Mesosphere Energetics and Dynamics (TIMED) satellite to examine migrating [*Wu et al.*, 2006, 2008a; *Xu et al.*, 2009] and nonmigrating [*Oberheide et al.*, 2005, 2006, 2007; *Wu et al.*, 2008b, 2009] tides at low and middle latitudes. Because TIDI measures horizontal winds from pole to pole every orbit, TIDI data were also used by *Iimura et al.* [2009] for an assessment of the nonmigrating semidiurnal tide over the Antarctic. This paper presents a similar analysis of the nonmigrating semidiurnal tide over the Arctic. Our analysis methods are described briefly in section 2. Results presented in section 3 include seasonal variations of the spatial structures of the nonmigrating semidiurnal tidal modes averaged over 60 day TIMED yaw intervals of the TIMED spacecraft. The observed dominant nonmigrating modes are found to be the W1, S0, and W3 modes. In section 4, the W1 mode over the Arctic is compared to that over the Antarctic. A discussion and summary of these results are presented in sections 5 and 6.

2. TIDI Wind Measurements and Analysis Approach

[8] Details of the TIDI instrument are described by *Yee et al.* [1999], *Killeen et al.* [1999, 2006], and *Skinner et al.* [2003]. TIDI employs four telescopes viewing O_2(0-0) emissions along 45° and 135° from the satellite orbit on each side and measuring horizontal line-of-sight (LOS) winds at altitudes from 70 to 120 km every 2.5 km. Recently, *Killeen et al.* [2006] introduced three modes of the TIDI measurements based on an O_2(0-0) band filter, p9 (763.78 nm), p15 (765.07 nm), and broadband (764.00 nm). Seasonal variations of the nonmigrating semidiurnal tidal structures over the Arctic presented in this paper are determined from the p9 mode processed at the University of Michigan because these data are continuous since 2002, except for a maximum data gap during 7 days in 2008. Availability of the TIDI data is described in detail online at (http://tidi.engin.umich.edu/).

[9] The TIMED spacecraft orbits the earth 15 to 16 times per day. Figure 1 shows a ground track of the TIMED spacecraft, in addition to locations and viewing directions of the TIDI measurements poleward of 40°N from 1432 to 1458 UT on day 105, 2008. Locations and directions of wind measurements by the four telescopes are shown in black (telescope 1), red (telescope 2), blue (telescope 3), and green (telescope 4). During the yaw interval from mid-March to mid-May, telescopes 3 and 4 measure winds poleward of 60°N in the rearward and forward directions of the spacecraft, respectively. The LOS winds are determined

every ~2 min. A time lag of ~10 min between forward and rearward measurements on each side of the satellite provides near "common volume" orthogonal LOS views from which horizontal vector winds are obtained. In Figure 1, telescopes 3 and 4 measured the winds at approximately 51.5°E and 234.3°E, which are equivalent to 1811 LT and 0622 LT, respectively.

[10] Ideally, vector horizontal winds can be determined with the LOS wind measurements using the two telescopes on either side of the spacecraft [*Wu et al.*, 2006]. However, each TIDI telescope has a different offset. Additionally, the TIDI telescopes are sensitive to solar radiation during measurements at high latitudes and the measurements contain noise having magnitudes that depend on the sensitivities of telescopes and strength of the solar radiation.

[11] We make two assumptions in our use of the TIDI data. We assume that the systematic errors in each telescope are constant with time and location. We also assume that the noise due to solar radiation varies slowly with time in each latitude circle. On the basis of these assumptions, the nonmigrating semidiurnal tidal modes over the Arctic were determined with the same method employed by *Iimura et al.* [2009] over the Antarctic. Over the course of the yaw interval the orbital plane precesses allowing TIDI to observe winds for roughly 12 h of LT of the ascending portion of the orbit and another 12 h of LT on the descending portion of the orbit.

[12] The measurement data were first collected in 5° latitude bins between 60°N and 85°N and a 3° bin from 85°N to 88°N and successive 3 day time-longitude running means were computed for each altitude and telescope separately. The daily LOS winds were differenced with these means, leaving residual time series. Because TIDI measures LOS winds at the same LT at different longitudes within each 3 day mean, the means include the migrating tides and the zonal mean. Thus, 3 day mean removal retains primarily the nonmigrating tides.

[13] LOS residuals during each yaw interval were further averaged to create hourly means of a composite day in a 24° longitude bin. Creating hourly means of a composite day largely removes traveling planetary waves such as the 2, 4, 10, 15, and 30 day waves. Thus the hourly means comprise primarily the nonmigrating tides. The hourly mean LOS residuals for two telescopes were next combined to determine residuals for the meridional and zonal components. Amplitudes and phases of the nonmigrating tidal modes were computed from a least squares fitting method to sinusoids with periods of 12 and 24 h and zonal wave numbers from westward-propagating 6 to eastward-propagating 6. While the zonal mean and migrating diurnal and semidiurnal tidal modes were obtained from this fitting, these values are not accurate for the reasons discussed above and are not presented. In our discussion, phase is referred to as a time lag of a maximum at longitude 0° and standard deviation of the estimates are referred to as uncertainties. Results are shown in an altitude range between 80 and 110 km because TIDI measures LOS winds continuously in this altitude range.

3. Results

3.1. Westward-Propagating Zonal Wave 1

[14] Amplitudes of the W1 mode in the meridional and zonal components at latitudes from 86.5°N to 60°N and altitudes from 80 to 110 km are shown in Figure 2 for six ~60 day yaw intervals averaged from 2002 to 2007. Yaw intervals are centered on 15 February, 15 April, 15 June, 15 August, 15 October, and 15 December each year due to the precession of the spacecraft orbit. The most striking features of the W1 amplitudes are the strong maxima occurring in both components during the yaw interval centered on 15 April. Mean amplitudes during this interval exhibit somewhat narrow maxima in altitude, with full width half maxima (FWHM) of ~15 km. Amplitude variations with altitude and latitude are nearly identical for the two components below ~100 km. However, the amplitude in the meridional component is larger (by a few ms^{-1}) at higher altitudes and all latitudes, with maximum amplitudes spanning latitudes from ~65 to 86.5°N. Maximum mean amplitudes are ~13 ms^{-1} at 105 km and 67.5°N for the meridional component and ~11 ms^{-1} at 102 km and 86.5°N for the zonal component. The mean amplitudes displayed here are surely less than the true maxima at the peak of the W1 response because of its confinement to a single 60 day yaw interval.

[15] The W1 mode exhibits significantly smaller and more spatially variable mean amplitudes during all of the other 60 day yaw intervals. In most cases, there is some spatial coherence in the amplitude distributions, see especially the meridional component during the June yaw interval and the zonal component during the October yaw interval. But the combination of smaller amplitudes and less coherent spatial responses suggests less coherent or persistent forcing dynamics and greater intermittency of the W1 mode during these times.

[16] Amplitudes and phases of the W1 mode during the April yaw interval are shown in Figures 3a and 3b as a function of latitude at 100 km and in Figures 3c and 3d as a function of altitude at 86.5°N. Amplitudes of the two components (Figure 3a) agree closely at higher latitudes and depart by ~2 ms^{-1} near 60°N. Phases of the two components (Figure 3b) are nearly constant with latitude, with each exhibiting less than a 1 h phase lag at 86.5°N relative to 60°N. The meridional phase leads the zonal phase by ~3 h at all latitudes. Vertical profiles of the amplitudes and phases (Figures 3c and 3d) reveal amplitude growth with altitude to maxima of ~13 ms^{-1} at ~100 km, with the meridional phase leading the zonal phase by ~3 h above 90 km indicating a mean vertical wavelength of ~37 km.

3.2. Standing Zonal Wave 0

[17] Spatial variations of S0 amplitudes for the same TIMED yaw intervals shown in Figure 2 for the W1 mode are displayed in Figure 4. This mode appears equatorward of 75°N during the February and April yaw intervals. During the February yaw interval, the S0 mode maximizes at ~72.5°N and 100–105 km in both components extending to lower altitudes in the meridional component. The structures of the meridional and zonal components are more similar during the April yaw interval. The meridional component appears above ~95 km, increasing in amplitude equatorward. The enhancement of the zonal component is somewhat more limited in altitude. At other times, the S0 mode exhibits smaller amplitudes, weaker spatial coherence, and localized maxima, suggesting weaker and more intermittent forcing during these intervals. Nevertheless, there is a small coherent response during the October yaw interval at lower latitudes
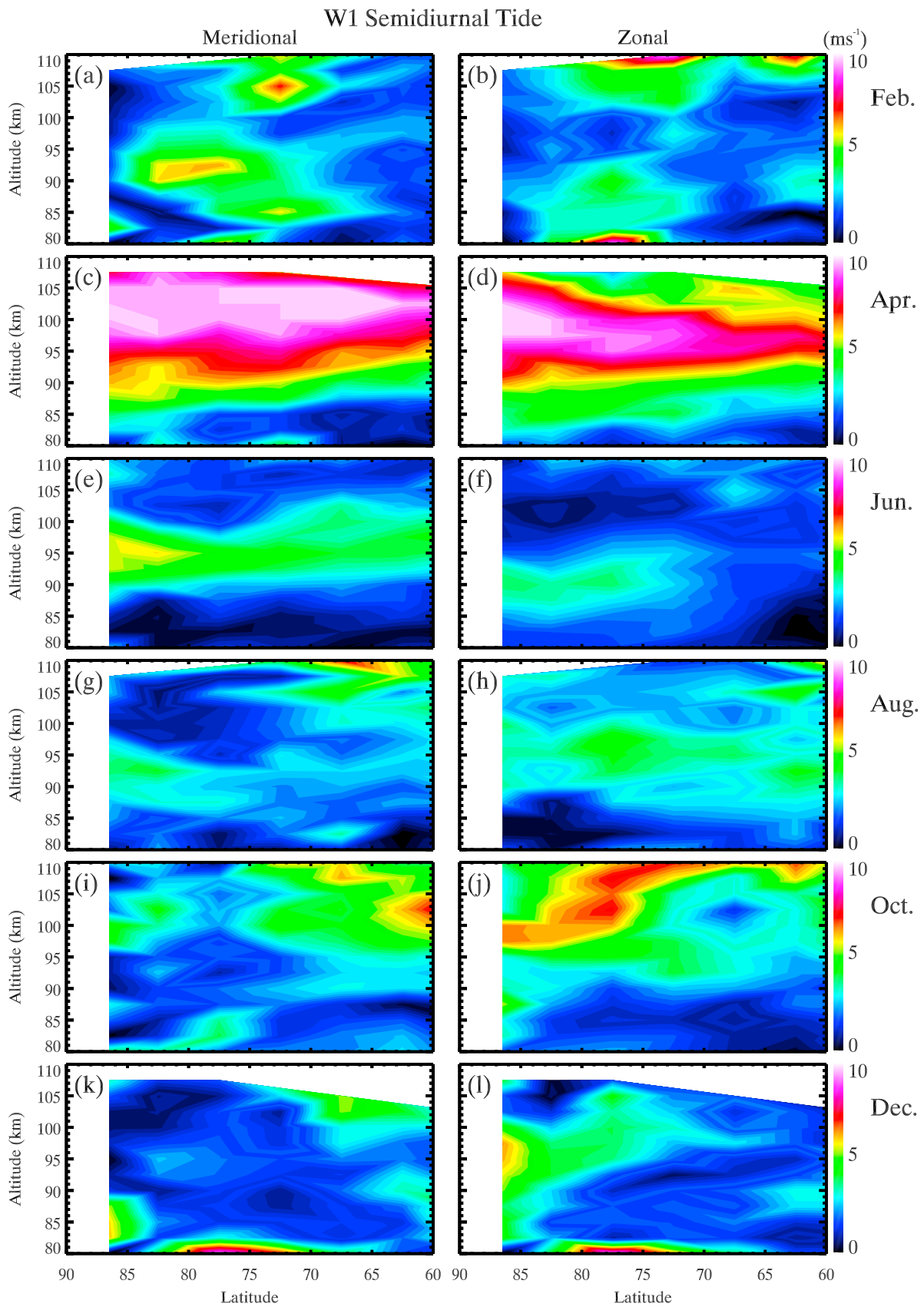
Figure 2.   Spatial structure of the W1 mode poleward of 60°N from 80 to 110 km over six yaw intervals. The (left) meridional and (right) zonal components are shown. Months indicate the centers of the 60 day analysis windows.
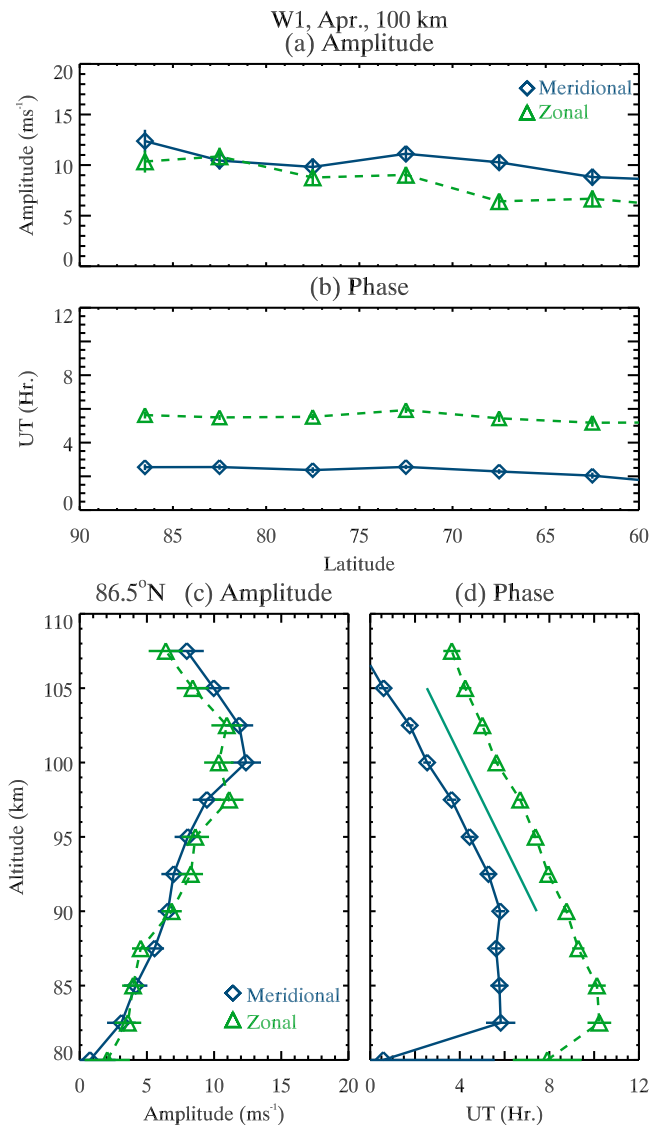
Figure 3. (a and b) Latitude variations at 100 km and (c and d) altitude variations at 86.5°N of amplitude and phase of the W1 mode from mid-March to mid-May. Blue diamonds (solid line) and green triangles (dashed line) are for the meridional and zonal components, respectively. Error bars indicate 1 standard deviation from the mean value. The line shown in Figure 3d indicates a vertical wavelength of 37 km.

and altitudes from ~95 to 100 km, indicating a semiannual oscillation.

[18] Figures 5a and 5b show latitude variations of S0 amplitudes and phases at 100 km during the April interval. A clear decrease in amplitude with increasing latitude is seen between 62.5°N and 82.5°N in both meridional and zonal components. The phases of the two components are nearly constant, exhibit ~3 h difference equatorward of ~80°N, and move to nearly the same phase poleward of ~80°N.

[19] Figures 5c and 5d show vertical profiles of the S0 amplitudes and phases at 62.5°N during the April yaw in-

terval. The amplitudes increase with altitude from ~90 to 97.5 km in the meridional component and from ~85 to 100 km in the zonal component. At altitudes between 90 and 105 km, both phases exhibit downward progression with the meridional phase leading the zonal by ~3 h. Vertical wavelengths in this altitude range are ~31 and ~37 km for the meridional and zonal components, respectively.

[20] Figures 5e and 5f are the same as Figures 5c and 5d, but for the October yaw interval. The S0 mode exhibits smaller vertical structures during the October yaw interval than during the April yaw interval, including amplitude growth with altitude to ~97.5 km and a decrease at higher altitudes. Similar phase variations to those during the April yaw interval are seen during the October yaw interval, but with longer vertical wavelengths.

3.3. Westward-Propagating Zonal Wave 3

[21] Spatial variations of W3 amplitudes for the same TIMED yaw intervals shown in Figure 2 for the W1 mode are displayed in Figure 6. The W3 amplitudes exhibit different apparent structures between the meridional and zonal components in all six yaw intervals, with typically larger amplitudes in the meridional component than in the zonal component. Amplitudes maximize during the February yaw interval in both components, but without consistent variations in altitude and latitude. This suggests intermittent forcing of this mode that may point to erratic or episodic source dynamics. The larger amplitudes and/or greater spatial coherence during the February and October yaw intervals nevertheless suggest that these are the dominant forcing periods of the W3 mode.

4. Comparisons of the W1 Over the Arctic and Antarctic

[22] *Iimura et al.* [2009] showed that the W1 mode over the Antarctic achieved maximum amplitudes during the yaw intervals from mid-September to mid-January. Amplitudes of the W1 mode over the Arctic and Antarctic are displayed for the seasonally comparable yaw intervals in Figure 7 to enable a comparison of the two responses. Significant differences in the two W1 responses are immediately apparent. These include the following: (1) larger amplitudes over the Antarctic than over the Arctic, (2) larger amplitude gradients with latitude (and altitude) over the Antarctic, (3) maximum amplitudes at lower altitudes over the Antarctic, and (4) a more extended seasonal response over the Antarctic. We discuss each of these differences in greater detail below.

[23] The W1 modes achieve maximum amplitudes ~50–70% larger over the Antarctic than over the Arctic during the corresponding yaw intervals, centered on 15 April over the Arctic and 15 October over the Antarctic. Maximum amplitudes are ~12 and 10 ms^{-1} over the Arctic and ~20 and 15 ms^{-1} over the Antarctic for the meridional and zonal components during the April and October yaw intervals, respectively. Differences of the W1 amplitude are even larger during the June (Arctic) and December (Antarctic) yaw intervals, with maximum amplitudes of ~6 and 4 ms^{-1} over the Arctic and ~13 and 16 ms^{-1} over the Antarctic for the meridional and zonal components, respectively. The larger amplitudes over the Antarctic during the December
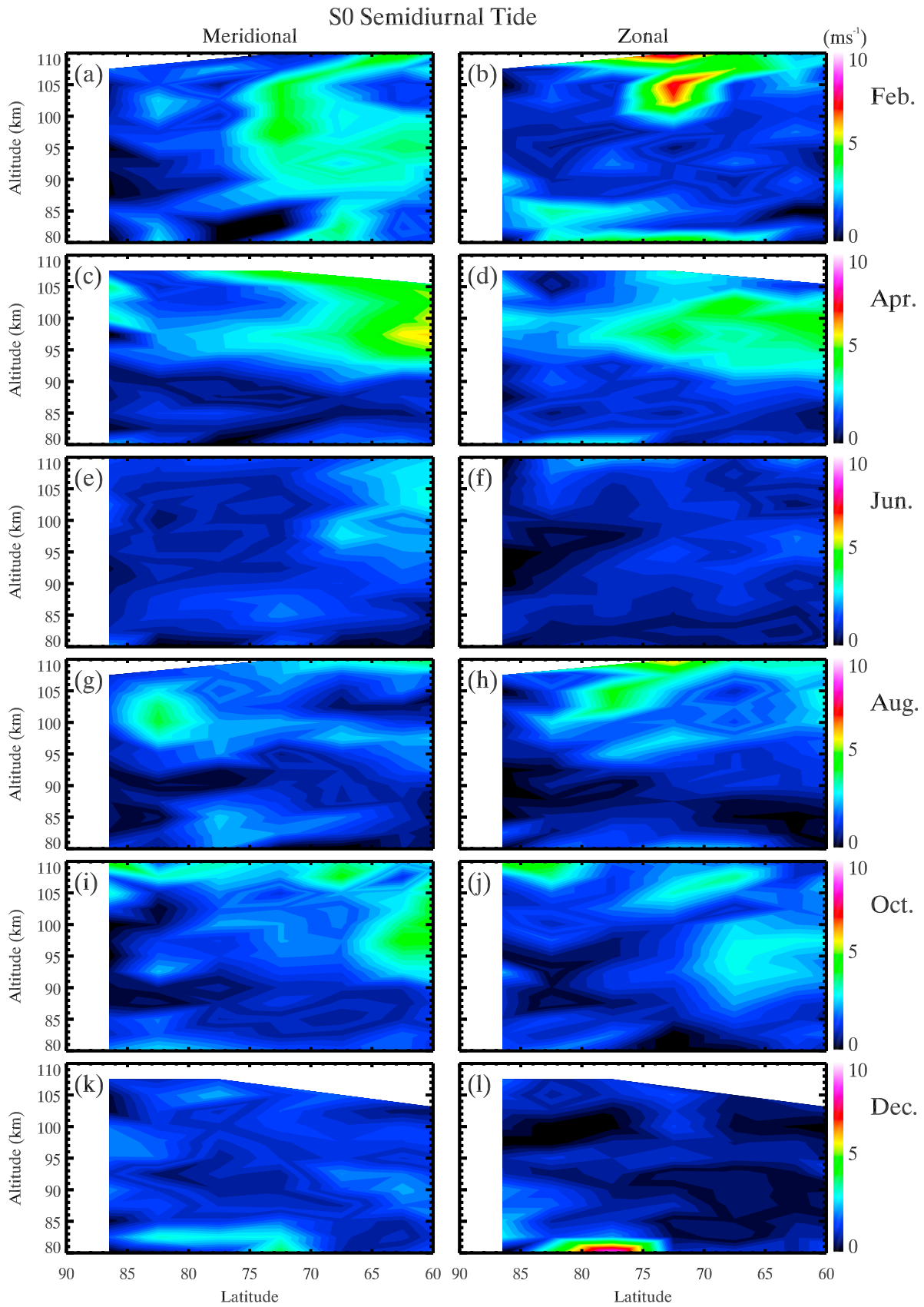
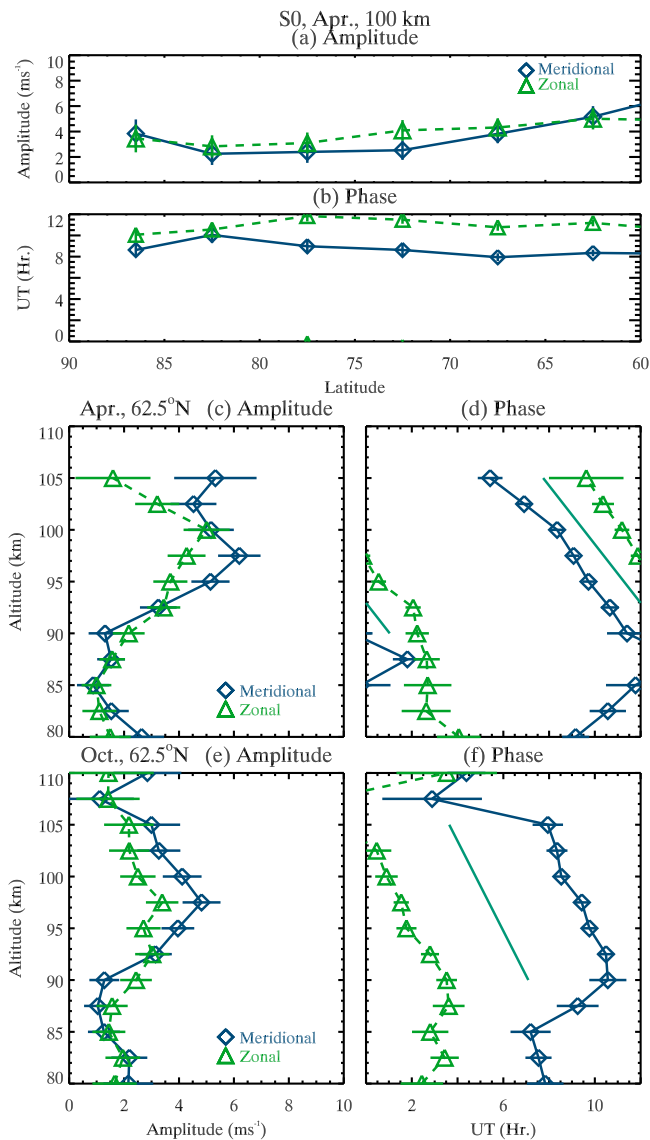**Figure 4.** As in Figure 2, but for the S0 mode.

Figure 5. As in Figure 3, but for the S0 mode. Altitude variations are at (c and d) 62.5°N from mid-March to mid-May and (e and f) from mid-September to mid-November, with mean vertical wavelengths of ~34 km (center) and ~74 km (bottom).

yaw interval indicate that the W1 response is more sustained than over the Arctic, likely due to more continuous sources.

[24] Amplitude gradients, in both latitude and altitude, are much more pronounced over the Antarctic than over the Arctic for all the yaw intervals displayed in Figure 7. While the relative amplitudes change over the Antarctic from October to December, they both exhibit pronounced polar maxima having sharp amplitude reductions spanning only a few kilometers above and below in each case.

[25] More detailed comparisons of the W1 altitude profiles at 86.5°N and 86.5°S during the April and October yaw intervals are shown in Figure 8 (top). A significant maximum amplitude in the meridional component is observed over the South Pole at 85 to 90 km. A smaller maximum amplitude at a higher altitude of 100 km occurs over the North Pole. The vertical profile of the W1 amplitude over

the North Pole is very similar between the meridional and zonal components. Over the South Pole, on the other hand, the maximum amplitude of the zonal component is much smaller than that of the meridional component though the altitudes of the maxima are same.

[26] Altitude variations of the W1 amplitudes at 86.5°N and S during the June and December yaw intervals are displayed in Figure 8 (bottom). The zonal components (Figure 8, right) have very similar altitude profiles between the South Pole and the North Pole, with maxima at 90–92.5 km, but differ by a factor of ~4 in amplitude. The meridional components (Figure 8, left) differ in their vertical structures as well as their amplitudes. The meridional W1 mode over the South Pole has a profile that closely resembles the zonal W1 mode, but with a slightly lower maximum altitude and a ~3 ms^{-1} smaller maximum amplitude. The meridional W1 mode over the North Pole, in contrast, exhibits a larger amplitude at a higher altitude than the zonal W1 mode, with a smaller amplitude than the meridional W1 mode over the South Pole at lower altitudes and a comparable amplitude at higher altitudes.

[27] Altitude profiles of the W1 phases are displayed in Figure 9. Similar phase profiles are observed over the North Pole in the meridional and zonal components with the meridional phase leading the zonal phase by ~3 h between 90 and 105 km. Thus, the vertical wavelengths are similar in the meridional and zonal components, ~34 and 40 km, respectively. The zonal phase over the South Pole shows a linear gradient with a vertical wavelength of ~40 km, which is nearly the same as for the zonal component over the North Pole. The meridional phase over the South Pole deviates from a linear gradient at ~100 km due to small amplitudes at these altitudes (see Figure 8a). Similar altitude profiles of the W1 phases are seen in the meridional (Figure 9c) and zonal (Figure 9d) components over the North and South Poles during the June and December yaw intervals. Vertical wavelengths are longer below ~90 km than between ~90 and 105 km over both poles, and appear to lengthen again at higher altitudes.

[28] Estimated latitude variations of the vertical wavelengths over the Arctic and Antarctic W1 modes during the June and December intervals are compared in Figure 10. Where amplitudes are sufficient to allow confident estimates, the vertical wavelengths exhibit similar trends over the Arctic and Antarctic, with shorter vertical wavelengths toward the poles.

5. Discussion

[29] On the basis of nonlinear interaction theory, nonmigrating tides can be excited by interactions between tides and planetary waves (PWs) [*Teitelbaum and Vial*, 1991; *Beard et al.*, 1999]. Theory suggests that the W1 semidiurnal tidal mode can be forced by the nonlinear interaction of the W2 semidiurnal tide and the stationary PW zonal wave number 1 (SPW1) [*Palo et al.*, 1998]. The growth of the W1 semidiurnal tide comes at the expense of the W2 semidiurnal tide or the SPW1. This was assessed by *Kamalabadi et al.* [1997] and *Baumgaertner et al.* [2006]. Modeling by *Angelats i Coll and Forbes* [2002] showed that this interaction in the winter hemisphere generates a W1 semidiurnal tide that propagates to the summer hemisphere.
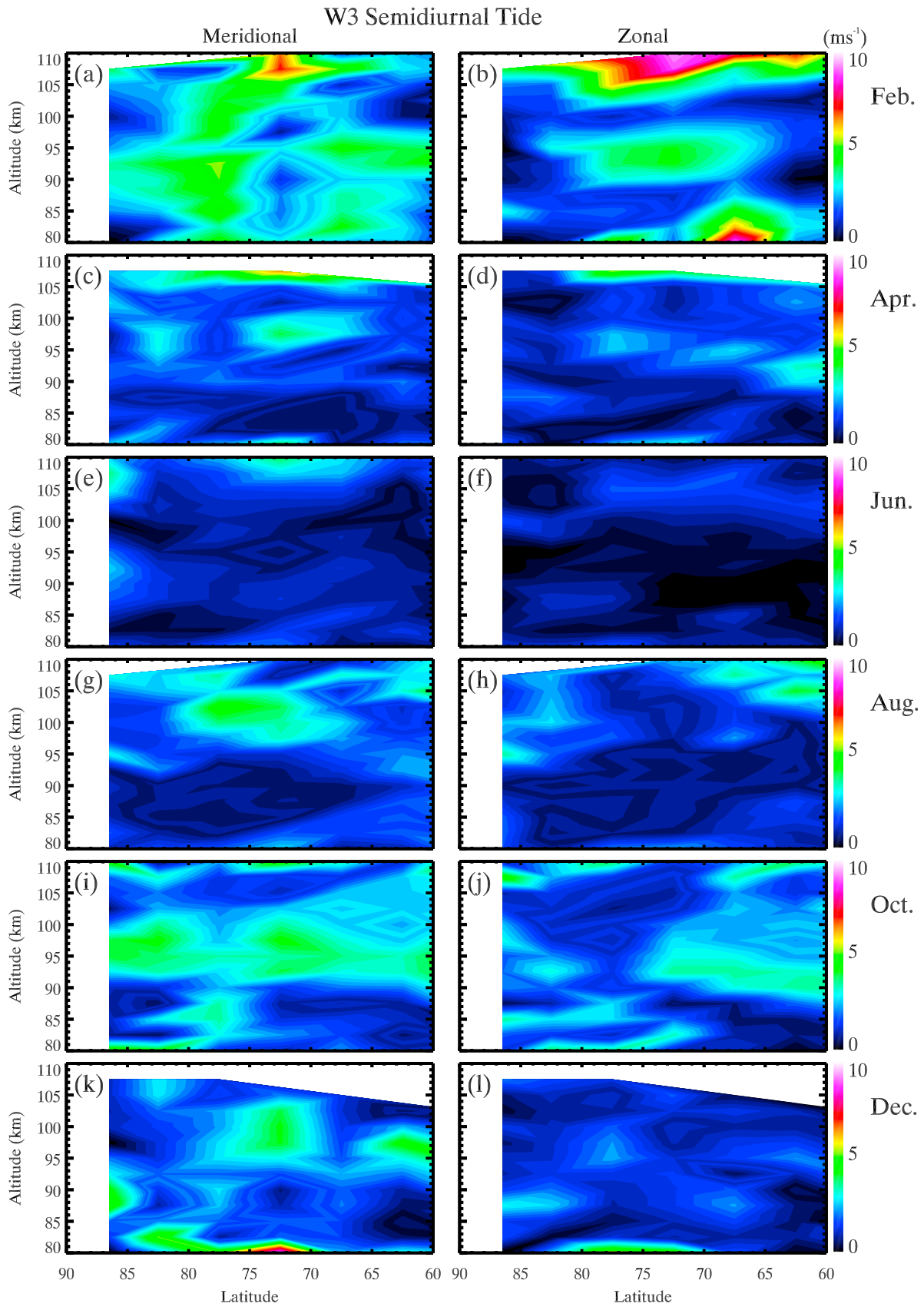
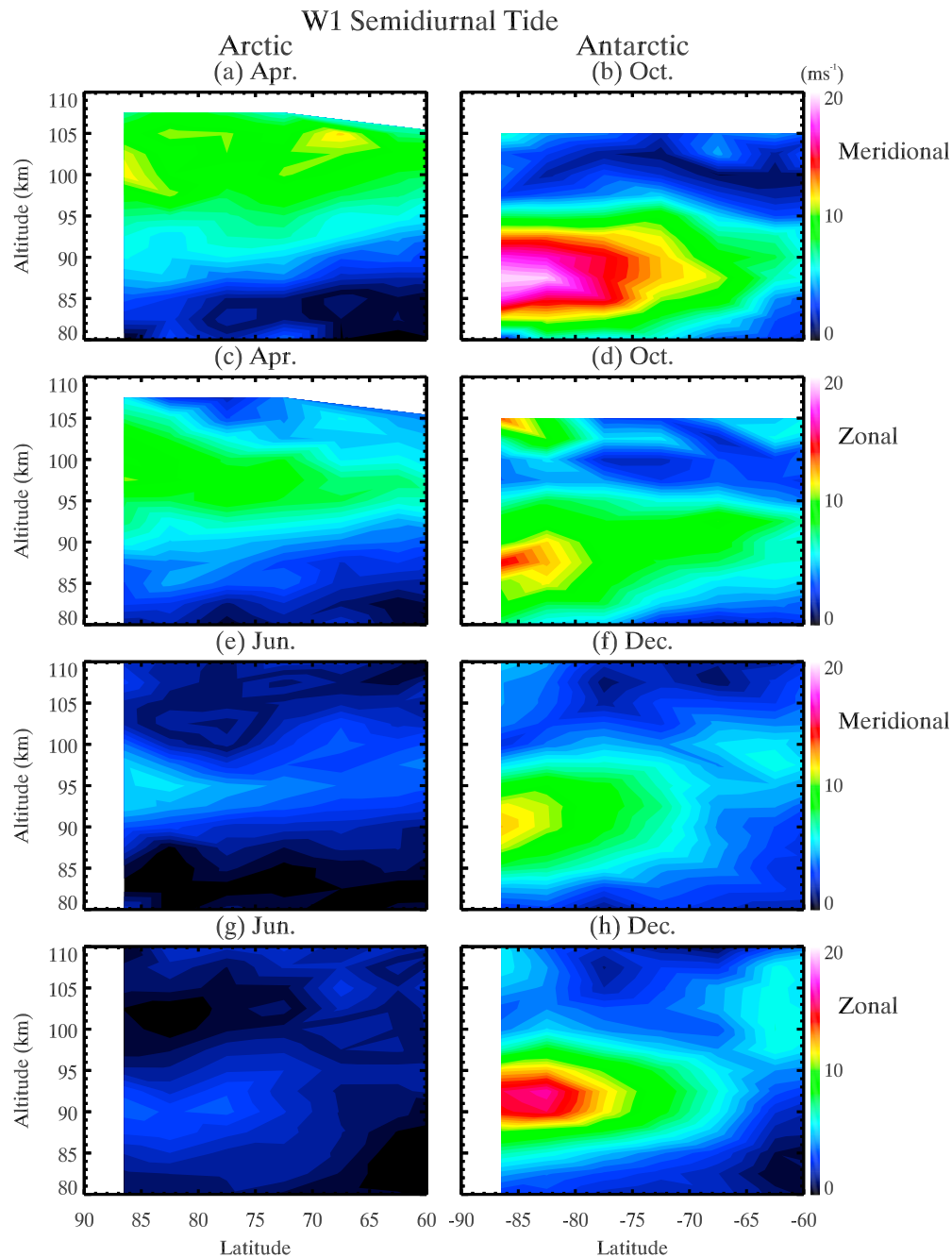**Figure 6.** As in Figure 2, but for the W3 mode.

Figure 7. Spatial structures of the W1 mode poleward of 60° from 80 to 110 km over two yaw intervals over the (left) Arctic and (right) Antarctic. Months indicate the centers of the 60 day analysis windows.

[30] Consistent with this theory, TIDI observes larger amplitudes of the W1 semidiurnal tide during Austral summer than at northern summer latitudes because the W2 semidiurnal tide and SPW1 in the stratosphere and lower mesosphere are larger at northern winter low and middle latitudes than at southern winter low and middle latitudes [*Hagan et al.*, 2001; *Zhang et al.*, 2006; *Pancheva et al.*, 2009]. The durations of the northern and southern W1 semidiurnal tidal events observed by TIDI suggest longer (shorter) intervals during which the W2 semidiurnal tide and the SPW1 are enhanced in the northern (southern) hemi-

sphere. The higher-altitude response of the W1 semidiurnal tide over the Arctic also suggests different conditions in the two cases.

[31] *Smith et al.* [2007] examined correlations between the SPW1 in the Southern Hemisphere determined from temperature and geopotential measurements by the Sounding the Atmosphere using Broadband Emission Radiometry (SABER) instrument aboard TIMED and the semidiurnal tide observed by a meteor radar at Esrange (68°N, 21°E), Sweden, and noted both correlated and uncorrelated intervals. They assumed that the semidiurnal tidal wind
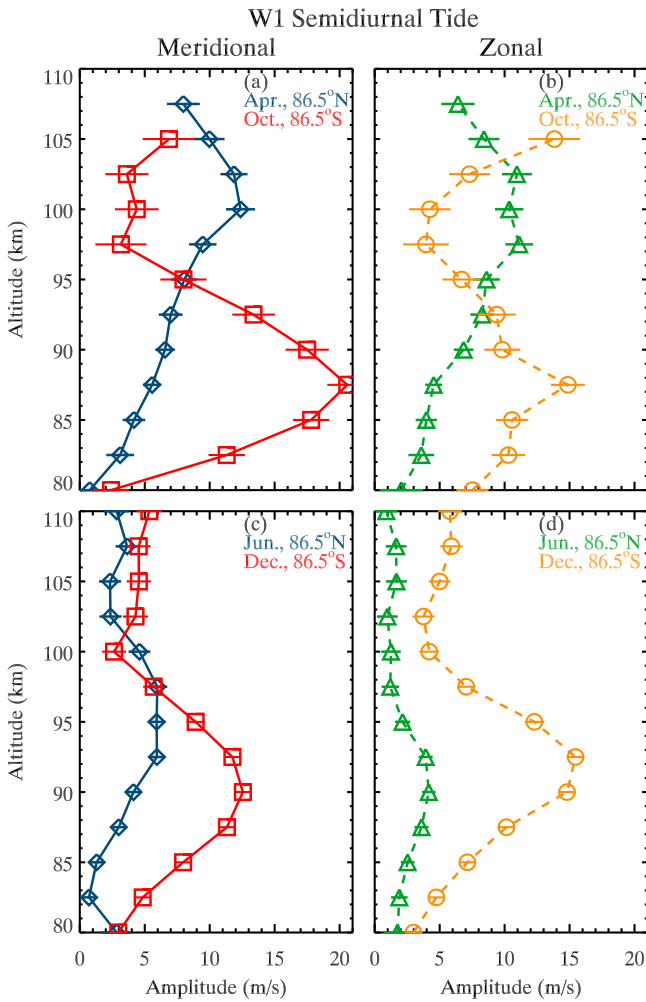
Figure 8. Altitude variations of the W1 amplitudes of the (left) meridional and (right) zonal components during two yaw intervals. Blue diamonds and green triangles are at 86.5°N, while red squares and yellow circles are at 86.5°S.

Figure 9. As in Figure 8, but for the phases.

field over Esrange was dominated by the W1 mode in their study. However, TIDI observes comparatively small amplitudes of the W1 mode over the Arctic, suggesting that the semidiurnal tide at Esrange is a mixture of the W2, W1, and possibly S0 modes having variable amplitudes.

[32] If the nonlinear interaction of the W1 semidiurnal tide and SPW1 can generate the S0 semidiurnal tide [*Angelats i Coll and Forbes*, 2002], the S0 mode may be enhanced when the W1 mode is enhanced. The W1 mode in Figure 2 and the S0 mode in Figure 4 are enhanced between 70°N and 75°N during the February yaw interval, maximize at approximately 100 km during the April yaw interval, and diminish during the June yaw interval. Additionally, these two modes are enhanced between 95 and 105 km and between 60°N and 65°N in the meridional component during the October yaw interval. Like the W1 mode, the S0 mode typically exhibits smaller amplitudes over the Arctic than over the Antarctic (see Figure 4 for the Arctic and Figure 11 of *Iimura et al.* [2009] for the Antarctic). These relations suggest that the S0 mode at high latitudes also arises from the nonlinear interaction between the W1 mode and SPW1.
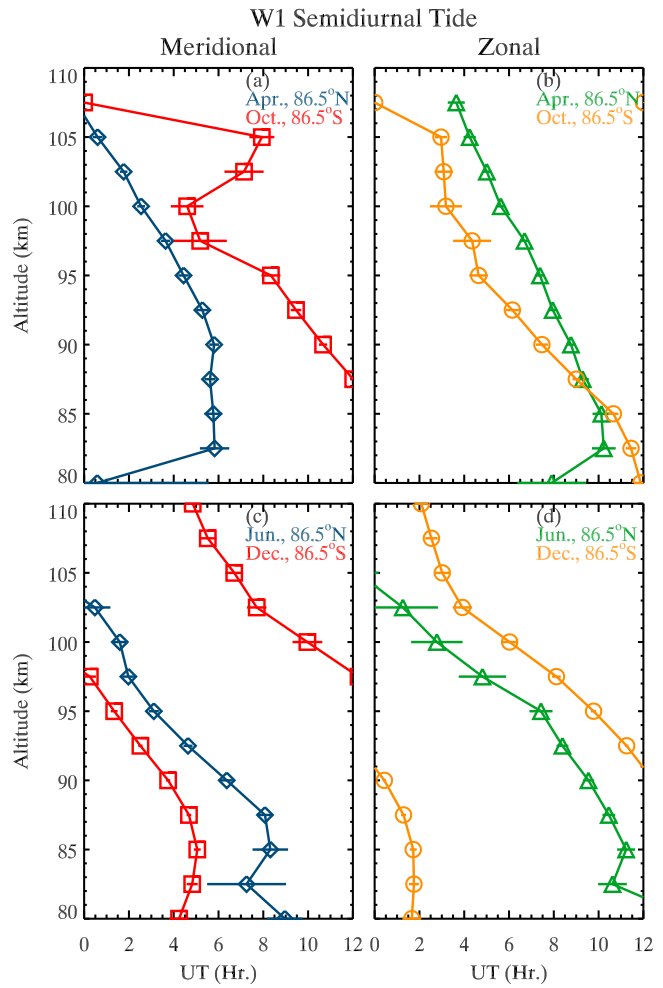
[33] The nonlinear interaction between the W2 semidiurnal tide and SPW1 is also expected to excite the W3 semidiurnal tide. However, Figure 6 shows that the W3 mode is not enhanced during the April yaw interval when the W1 and S0
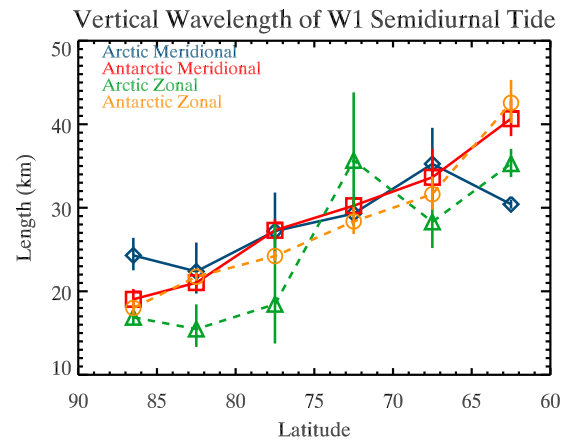

Figure 10. Latitude variations of the vertical wavelengths of the W1 mode. Colors and symbols are as indicated in Figure 8.

modes are, suggesting possibly different forcing mechanisms between the W1 and W3 modes.

[34] Simulations with the Middle Atmosphere Circulation Model at Kyushu University (MACMKU) by *Yamashita et al.* [2002] suggested that the amplitude of the W1 semidiurnal tide increases with altitude, maximizing at ~105 km poleward of 60°N with amplitudes >20 ms^{-1} in July and with a maximum at ~86°N and ~100 km in August. TIDI observations, on the other hand, show that the W1 mode over the Arctic is enhanced at 100 km during the April yaw interval and moderately between 90 and 95 km during the June yaw interval. The extended Canadian Middle Atmosphere Model (CMAM) simulation described by *Du et al.* [2007] suggests an amplitude of the W1 mode ~6 ms^{-1} at 95 km poleward of 60°N in June. On the other hand, the Numerical Spectral Mode (NSM) by *Mayr et al.* [2005] suggests that the W1 mode is >24 ms^{-1} above 95 km in the vicinity of the North Pole in January and February and ~48 ms^{-1} at 110 km. Thus, there are major differences in the predictions of the W1 semidiurnal tidal amplitudes, altitudes, and times of maxima among the available models.

[35] TIDI observations, in contrast, suggest that the W1 mode over the Arctic maximizes at ~13 ms^{-1} near 100 km during the April yaw interval and between 90 and 95 km during June yaw interval. So while the three models span the observed amplitudes and are reasonably close in the altitudes of the peak responses, their seasonal variations typically depart significantly from the TIDI observations. Seasonal and amplitude differences between the TIDI measurements and the three models may arise, in part, from the longer averaging employed for the TIDI estimates (60 days) compared to the monthly means quoted for the models. This is particularly true if the W1 semidiurnal tide occurrences are somewhat transient and/or exhibit significant phase variability within any 60 day yaw interval. There are also differences in spatial structure and temporal evolution on timescales longer than the 60 day yaw interval that cannot be accounted for by different temporal averaging, however. Such differences may arise due to parameterizations in the various models, e.g., of gravity wave drag effects, that fail to adequately describe these effects in the atmosphere [*Hagan et al.*, 1997; *McLandress*, 1998].

[36] Additionally, effects of interannual variations in the nonmigrating semidiurnal tide at high latitudes noted by *Baumgaertner et al.* [2006], *Hibbins and Jarvis* [2007], *Portnyagin et al.* [1998], and *Riggin et al.* [1999] need to be considered in comparing measurements and model predictions. The seasonal structures of the nonmigrating semidiurnal tidal modes presented here are obtained as means of the 5 year measurements from 2002 to 2007. The results cannot describe linear trends [*Merzlyakov et al.*, 2009], effects of the quasi-biennial oscillation (QBO) [*Hagan et al.*, 1992; *Hibbins et al.*, 2009], or of varying solar radiation [*Baumgaertner et al.*, 2005; *Fraser et al.*, 1989; *Fraser*, 1990]. Interannual variations of the tidal wind field are also specifically observed by TIDI [*Wu et al.*, 2008a, 2008b]. Analysis of the interannual variations of the nonmigrating semidiurnal tides is beyond the scope of this effort, however, and will be a subject of future work.

[37] *Riggin et al.* [2003] compared the semidiurnal tide determined from ground-based radar wind measurements at Andenes (69°N, 16°E), Norway, Poker Flat (65°N, 147°W), Alaska, and Rothera (68°S, 68°W) and Davis (69°S, 78°E), Antarctica. Their results exhibit a maximum >25 ms^{-1} in September over Andenes. These longitudinal differences indicate influences of the nonmigrating tidal modes on the overall tidal amplitudes at any one site, and provide some hint of the nonmigrating tidal amplitude(s). But they provide no quantitative information on these amplitudes or their modal composition without a thorough assessment and decomposition of the tidal fields, which is impossible with ground-based measurements at only a few sites. Because TIDI measurements in September straddle two yaw intervals, it is not possible to identify a maximum amplitude occurring only during September. Even a transient maximum or significant phase variability would cause an underestimate. Additionally, our TIDI measurements were averaged over 5 years, and are thus insensitive to interannual variability. Thus, comparisons of the nonmigrating semidiurnal tidal modes observed by TIDI with ground-based measurements of the full semidiurnal tidal field at any one site cannot resolve ambiguities in tidal composition without substantially more (and coincident) data.

[38] The total semidiurnal tide described by *Riggin et al.* [2003] over the Antarctic, in contrast to the Arctic, does not exhibit a clear maximum. Thus, TIDI observations of a clear maximum during the October yaw interval imply that the nonmigrating semidiurnal tide, comprising primarily the W1 mode, is comparable in amplitude to the W2 mode over the Antarctic. These observations also suggest that the W2 mode over the Antarctic is smaller than the W2 mode over the Arctic, as predicted by the Global-Scale Wave Model (GSWM) [*Hagan et al.*, 2001], and perhaps contributes to an easier assessment of the nonmigrating semidiurnal tides over the Antarctic. In principle, it should be possible to estimate seasonal structures of the migrating semidiurnal tide defined from ground-based wind measurements and of the nonmigrating semidiurnal tide defined from TIDI observations for the same periods in order to define the full tidal motion field. Because tidal motions exhibit significant spatial and temporal variability, however, it will likely not be possible to assess the full tidal motion field on much shorter timescales without much more comprehensive (likely space-based) observations. Nevertheless, improving temporal resolution of the full tidal field employing joint analyses of satellite and ground-based wind measurements will likely yield benefits in future studies.

6. Summary

[39] This paper presents the first assessment of the seasonal variations of the nonmigrating semidiurnal tidal structure comprising westward-propagating zonal wave numbers 1 and 3 and standing zonal wave number 0 determined from TIDI wind measurements over the Arctic.

[40] Enhancements of the W1 mode were observed before summer solstice from mid-March to mid-May above 95 km in both meridional and zonal components. The zonal component exhibited clearer latitudinal variations in amplitude than the meridional component, increasing poleward to ~10 ms^{-1} near the North Pole. The phase structure of the W1 mode was nearly constant with latitude for both meridional

and zonal components. Altitude variations of the phases revealed downward progression during summer with a vertical wavelength of ~37 km. The W1 mode was also enhanced slightly from mid-September to mid-November, suggesting a semiannual oscillation.

[41] Enhancements of the S0 mode were observed from mid-March to mid-May. However, this mode appeared equatorward of 75°N, with a decreasing amplitude toward the North Pole throughout the year. During the two yaw intervals from mid-March to mid-May and from mid-September to mid-November, altitude profiles of the phases revealed downward progression with nearly the same vertical wavelength in the meridional and zonal components, but longer wavelengths from mid-September to mid-November than from mid-March to mid-May. The S0 mode showed a semiannual oscillation at 60°N, more clearly in the meridional component than in the zonal component. The W3 mode was observed from mid-January to mid-March.

[42] The amplitude of the W1 mode was greater over the Antarctic during Austral summer than over the Arctic in northern summer, and also enhanced at lower altitudes and over longer intervals. The amplitude of the W1 mode showed larger latitudinal variations over the Antarctic. Vertical wavelengths of the summer W1 modes were shorter poleward over both the Arctic and Antarctic.

References

Angelats i Coll, M., and J. M. Forbes (2002), Nonlinear interactions in the upper atmosphere: The $s = 1$ and $s = 3$ nonmigrating semidiurnal tides, *J. Geophys. Res.*, *107*(A8), 1157, doi:10.1029/2001JA900179.

Aso, T. (2003), An overview of the terdiurnal tide observed by polar radars and optics, *Adv. Pol. Upper Atmos. Res.*, *17*, 167–176.

Avery, S. K., R. A. Vincent, A. Phillips, A. H. Manson, and G. J. Fraser (1989), High-latitude tidal behavior in the mesosphere and lower thermosphere, *J. Atmos. Terr. Phys.*, *51*, 595–608.

Baumgaertner, A. J. G., A. J. McDonald, G. J. Fraser, and G. E. Plank (2005), Long-term observations of mean winds and tides in the upper mesosphere and lower thermosphere above Scott Base, Antarctica, *J. Atmos. Sol. Terr. Phys.*, *67*, 1480–1496, doi:10.1016/j.jastp.2005.07.018.

Baumgaertner, A. J. G., M. J. Jarvis, A. J. McDonald, and G. J. Fraser (2006), Observations of the wavenumber 1 and 2 components of the semi-diurnal tide over Antarctica, *J. Atmos. Sol. Terr. Phys.*, *68*, 1195–1214, doi:10.1016/j.jastp.2006.03.001.

Beard, A. G., N. J. Mitchell, P. J. S. Williams, and M. Kunitake (1999), Non-linear interactions between tides and planetary waves resulting in periodic tidal variability, *J. Atmos. Terr. Phys.*, *61*, 363–376.

Chapman, S., and R. Lindzen (1970), *Atmospheric tides: Thermal and Gravitational*, Reidel, Dordrecht, Netherlands.

Du, J., W. E. Ward, J. Oberheide, T. Nakamura, and T. Tsuda (2007), Semidiurnal tides from the extended Canadian Middle Atmosphere Model (CMAM) and comparisons with TIMED Doppler interferometer (TIDI) and meteor radar observations, *J. Atmos. Sol. Terr. Phys.*, *69*, 2159–2202, doi:10.1016/j.jastp.2007.07.014.

Fisher, G. M., R. J. Niciejewski, T. L. Killeen, W. A. Gault, G. G. Shepherd, S. Brown, and Q. Wu (2002), Twelve-hour tides in the winter northern polar mesosphere and lower thermosphere, *J. Geophys. Res.*, *107*(A8), 1211, doi:10.1029/2001JA000294.

Forbes, J. M. (1982a), Atmospheric tides: 1. Model description and results for the solar diurnal component, *J. Geophys. Res.*, *87*, 5222–5240.

Forbes, J. M. (1982b), Atmospheric tides: 2. The solar and lunar semidiurnal components, *J. Geophys. Res.*, *87*, 5241–5252.

Forbes, J. M. (1995), *Tidal and planetary waves*, in *The Upper Mesosphere and Lower Thermosphere: A Review of Experiment and Theory*, Geophys. Monogr. Ser., vol. 87, AGU, Washington, D. C.

Forbes, J. M., N. A. Makarov, and Y. I. Portnyagin (1995), First results from the meteor radar at South Pole: A large 12-hour oscillation with zonal wavenumber one, *Geophys. Res. Lett.*, *22*, 3247–3250, doi:10.1029/95GL03370.

Forbes, J. M., S. E. Palo, X. Zhang, Y. I. Portnyagin, N. A. Makarov, and E. G. Merzlyakov (1999a), Lamb waves in the lower thermosphere: Observational evidence and global consequences, *J. Geophys. Res.*, *104*, 17,107–17,116, doi:10.1029/1999JA900044.

Forbes, J. M., I. Y. Portnyagin, N. A. Makarov, S. E. Palo, E. G. Merzlyakov, and X. Zhang (1999b), Dynamics of the lower thermosphere over South Pole from meteor radar wind measurements, *Earth Planets Space*, *51*, 611–620.

Fraser, G. J. (1990), Long-term variations in mid-latitude Southern Hemisphere mesospheric winds, *Adv. Space Res.*, *10*, 247–250, doi:10.1016/0273-1177(90)90039-3.

Fraser, G. J., Y. I. Portnyagin, J. M. Forbes, R. A. Vincent, I. A. Lysenko, and N. A. Makarov (1995), Diurnal tide in the Antarctic and Arctic mesosphere/lower thermosphere regions, *J. Atmos. Terr. Phys.*, *57*, 383–393.

Fraser, G. K., R. A. Vincent, A. H. Manson, C. E. Meek, and R. R. Clark (1989), Inter-annual variability of tides in the mesosphere and lower thermosphere, *J. Atmos. Terr. Phys.*, *7*, 555–567.

Hagan, M. E., and J. M. Forbes (2002), Migrating and nonmigrating diurnal tides in the middle and upper atmosphere excited by tropospheric latent heat release, *J. Geophys. Res.*, *107*(D24), 4754, doi:10.1029/2001JD001236.

Hagan, M. E., and J. M. Forbes (2003), Migrating and nonmigrating semidiurnal tides in the upper atmosphere excited by tropospheric latent heat release, *J. Geophys. Res.*, *108*(A2), 1062, doi:10.1029/2002JA009466.

Hagan, M. E., F. Vial, and J. M. Forbes (1992), Variability in the upward propagating semidiurnal tide due to effects of QBO in the lower atmosphere, *J. Atmos. Terr. Phys.*, *54*, 1465–1474.

Hagan, M. E., J. L. Chang, and S. K. Avery (1997), Global-scale wave model estimates of nonmigrating tidal effects, *J. Geophys. Res.*, *102*, 16,439–16,452, doi:10.1029/97JD01269.

Hagan, M. E., R. G. Roble, and J. Hackney (2001), Migrating thermospheric tides, *J. Geophys. Res.*, *106*, 12,739–12,752, doi:10.1029/2000JA000344.

Hernandez, G., G. J. Fraser, and R. W. Smith (1993), Mesospheric 12-hour oscillation near South Pole, Antarctica, *Geophys. Res. Lett.*, *20*, 1787–1790.

Hibbins, R. E., and M. J. Jarvis (2007), A long-term comparison of wind and tide measurements in the upper mesosphere recorded with an imaging Doppler interferometer and SuperDARN radar at Halley, Antarctica, *Atmos. Chem. Phys. Discuss.*, *7*, 6573–6601.

Hibbins, R. E., M. J. Jarvis, and E. A. K. Ford (2009), Quasi-biennial oscillation influence on long-period planetary waves in the Antarctic upper mesosphere, *J. Geophys. Res.*, *114*, D09109, doi:10.1029/2008JD011174.

Hocking, W. K. (2001), Middle atmosphere dynamical studies at Resolute Bay over a full representative year: Mean winds, tides, and special oscillations, *Radio Sci.*, *36*, 1795–1822, doi:10.1029/2000RS001003.

Hoffmann, P., W. Singer, D. Keuer, W. K. Hocking, M. Kunze, and Y. Murayama (2007), Latitudinal and longitudinal variability of mesospheric winds and temperatures during stratospheric warming events, *J. Atmos. Sol. Terr. Phys.*, *69*, 2355–2366, doi:10.1016/j.jastp.2007.06.010.

Iimura, H., S. E. Palo, Q. Wu, T. L. Killeen, S. C. Solomon, and W. R. Skinner (2009), Structure of the nonmigrating semidiurnal tide above Antarctica observed from the TIMED Doppler Interferometer, *J. Geophys. Res.*, *114*, D11102, doi:10.1029/2008JD010608.

Kamalabadi, F., J. M. Forbes, N. M. Makarov, and Y. I. Portnyagin (1997), Evidence for nonlinear coupling of planetary waves and tides in the Antarctic mesopause, *J. Geophys. Res.*, *102*, 4437–4446, doi:10.1029/96JD01996.

Kato, S. (1980), *Dynamics of the Upper Atmosphere*, Springer, New York.

Killeen, T. L., et al. (1999), TIMED Doppler interferometer (TIDI), *Proc. SPIE*, *3756*, 289–301.

Killeen, T. L., Q. Wu, S. C. Solomon, D. A. Ortland, W. R. Skinner, R. J. Niciejewski, and D. A. Gell (2006), TIMED Doppler Interferometer: Overview and recent results, *J. Geophys. Res.*, *111*, A10S01, doi:10.1029/2005JA011484.

Kishore, P., S. P. Namboothiri, K. Igarashi, Y. Murayama, and B. J. Watkins (2002), MF radar observations of mean winds and tides over Poker Flat, Alaska (65.1°N, 147.5°W), *Ann. Geophys.*, *20*, 679–690.

Lau, E. M., S. K. Avery, J. P. Avery, S. E. Palo, and N. A. Makarov (2006), Tidal analysis of meridional winds at the South Pole using a VHF interferometric meteor radar, *J. Geophys. Res.*, *111*, D16108, doi:10.1029/2005JD006734.

Lindzen, R. A. (1990), *Dynamics in Atmospheric Physics*, Cambridge Univ. Press, New York.

Mayr, H. G., J. G. Mengel, E. R. Talaat, H. S. Porter, and K. L. Chan (2005), Mesopsheric non-migrating tides generated with planetary waves: I. Characteristics, *J. Atmos. Sol. Terr. Phys.*, 67, 959–980.

McLandress, C. (1998), On the importance of gravity waves in the middle atmosphere and their parameterization in general circulation models, *J. Atmos. Terr. Phys.*, 60, 1357–1383.

McLandress, C., G. G. Shepherd, and B. H. Solheim (1996), Satellite observations of thermospheric tides: Results from the Wind Imaging Interferometer on UARS, *J. Geophys. Res.*, 101, 4093–4114, doi:10.1029/95JD03359.

Merzlyakov, E. G., Y. I. Portnyagin, N. A. Makarov, J. Forbes, and S. Palo (2005), Eastward-propagating day-to-day wind oscillations in the northern polar mesosphere/lower thermosphere, *Atmos. Oceanic Phys.*, 41, 92–104.

Merzlyakov, E. G., D. J. Murphy, R. A. Vincent, and Y. I. Portnyagin (2009), Long-term tendencies in the MLT prevailing winds and tides over Antarctica as observed by radars at Molodezhnaya, Mawson and Davis, *J. Atmos. Sol. Terr. Phys.*, 71, 21–32, doi:10.1016/j.jastp.2008.09.024.

Mitchell, N. J., D. Pancheva, H. R. Middleton, and M. E. Hagan (2002), Mean winds and tides in the Arctic mesosphere and lower thermosphere, *J. Geophys. Res.*, 107(A1), 1004, doi:10.1029/2001JA900127.

Miyahara, S., and Y. Miyoshi (1997), Migrating and non-migrating atmospheric tides simulated by a middle atmosphere general circulation model, *Adv. Space Res.*, 20, 1201–1207.

Murphy, D. J., et al. (2006), A climatology of tides in the Antarctic mesosphere and lower thermosphere, *J. Geophys. Res.*, 111, D23104, doi:10.1029/2005JD006803.

Nozawa, S., et al. (2005), Mean winds, tides, and quasi-2 day wave in the polar lower thermosphere observed in European Incoherent Scatter (EISCAT) 8 day run data in November 2003, *J. Geophys. Res.*, 110, A12309, doi:10.1029/2005JA011128.

Oberheide, J., Q. Wu, D. A. Ortland, T. L. Killeen, M. E. Hagan, R. G. Roble, R. J. Niciejewski, and W. R. Skinner (2005), Non-migrating diurnal tides as measured by the TIMED Doppler interferometer: Preliminary results, *Adv. Space Res.*, 35, 1911–1917, doi:10.1016/j.asr.2005.01.063.

Oberheide, J., Q. Wu, T. L. Killeen, M. E. Hagan, and R. G. Roble (2006), Diurnal nonmigrating tides from TIMED Doppler Interferometer wind data: Monthly climatologies and seasonal variations, *J. Geophys. Res.*, 111, A10S03, doi:10.1029/2005JA011491.

Oberheide, J., Q. Wu, T. L. Killeen, M. E. Hagan, and R. G. Roble (2007), A climatology of nonmigrating semidiurnal tides from TIMED Doppler Interferometer (TIDI) wind data, *J. Atmos. Sol. Terr. Phys.*, 69, 2203–2218, doi:10.1016/j.jastp.2007.05.010.

Palo, S. E., Y. I. Portnyagin, J. M. Forbes, N. A. Makarov, and E. G. Merzlyakov (1998), Transient eastward-propagating long-period waves observed over the South Pole, *Ann. Geophys.*, 16, 1486–1500.

Pancheva, D., P. Mukhtarov, B. Andonov, N. J. Mitchell, and J. M. Forbes (2009), Planetary waves observed by TIMED/SABER in coupling the stratosphere-mesosphere-lower thermosphere during the winter of 2003/2004: Part 2—Altitude and latitude planetary wave structure, *J. Atmos. Sol. Terr. Phys.*, 71, 75–87, doi:10.1016/j.jastp.2008.09.027.

Portnyagin, Y. I., J. M. Forbes, G. J. Fraser, R. A. Vincent, S. K. Avery, I. A. Lysenko, and N. A. Makarov (1993), Dynamics of the Antarctic and Arctic mesosphere and lower thermosphere regions—II. The semidiurnal tide, *J. Atmos. Terr. Phys.*, 55, 843–855.

Portnyagin, Y. I., J. M. Forbes, N. A. Makarov, E. G. Merzlyakov, and S. Palo (1998), The summertime 12-h wind oscillation with zonal wavenumber s = 1 in the lower thermosphere over the South Pole, *Ann. Geophys.*, 16, 828–837.

Riggin, D. M., D. C. Fritts, M. J. Jarvis, and G. O. L. Jones (1999), Spatial structure of the 12-hour wave in the Antarctic as observed by radar, *Earth Planets Space*, 51, 621–628.

Riggin, D. M., C. K. Meyer, D. C. Fritts, M. J. Jarvis, Y. Murayama, W. Singer, R. A. Vincent, and D. J. Murphy (2003), MF radar observations of seasonal variability of semidiurnal motions in the mesosphere at high northern and southern latitudes, *J. Atmos. Terr. Phys.*, 65, 483–493.

Singer, W., R. Latteck, P. Hoffman, B. P. Williams, D. C. Fritts, Y. Murayama, and K. Sakanoi (2005), Tides near the Arctic summer mesopause during the MaCWAVE/MIDAS summer program, *Geophys. Res. Lett.*, 32, L07S90, doi:10.1029/2004GL021607.

Skinner, W. R., et al. (2003), Operational performance of the TIMED Doppler Interferometer (TIDI), *Proc. SPIE*, 5157, 47–57, doi:10.1117/12.503727.

Smith, A. K., D. V. Pancheva, N. J. Mitchell, D. R. Marsh, J. M. Russell, and M. G. Mlynczak (2007), A link between variability of the semidiurnal tide and planetary waves in the opposite hemisphere, *Geophys. Res. Lett.*, 34, L07809, doi:10.1029/2006GL028929.

Teitelbaum, H., and F. Vial (1991), On tidal variability induced by nonlinear interaction with planetary waves, *J. Geophys. Res.*, 96, 14,169–14,178.

Volland, H. (1988), *Atmospheric Tidal and Planetary Waves*, Kluwer Acad., Boston, Mass.

Wu, Q., T. L. Killeen, S. Nozawa, D. McEwen, W. Guo, and S. C. Solomon (2003), Observations of mesospheric neutral wind 12-hour wave in the Northern Polar Cap, *J. Atmos. Terr. Phys.*, 65, 971–978.

Wu, Q., T. L. Killeen, D. A. Ortland, S. C. Solomon, R. D. Gablehouse, R. M. Johnson, W. R. Skinner, R. J. Niciejewski, and S. J. Franke (2006), TIMED Doppler interferometer (TIDI) observations of migrating diurnal and semidiurnal tides, *J. Atmos. Sol. Terr. Phys.*, 68, 408–417, doi:10.1016/j.jastp.2005.02.031.

Wu, Q., et al. (2008a), Global distribution and interannual variations of mesospheric and lower thermospheric neutral wind diurnal tide: 1. Migrating tide, *J. Geophys. Res.*, 113, A05308, doi:10.1029/2007JA012542.

Wu, Q., et al. (2008b), Global distribution and interannual variations of mesospheric and lower thermospheric neutral wind diurnal tide: 2. Nonmigrating tide, *J. Geophys. Res.*, 113, A05309, doi:10.1029/2007JA012543.

Wu, Q., S. C. Solomon, Y.-H. Kuo, T. L. Killeen, and J. Xu (2009), Spectral analysis of ionospheric electron density and mesospheric neutral wind diurnal nonmigrating tides observed by COSMIC and TIMED satellites, *Geophys. Res. Lett.*, 36, L14102, doi:10.1029/2009GL038933.

Xu, J., A. K. Smith, H.-L. Liu, W. Yuan, Q. Wu, G. Jiang, M. G. Mlynczak, J. M. Russell, and S. J. Franke (2009), Seasonal and quasi-biennial variations in the migrating diurnal tide observed by Thermosphere, Ionosphere, Mesosphere, Energetics and Dynamics (TIMED), *J. Geophys. Res.*, 114, D13107, doi:10.1029/2008JD011298.

Yamashita, K., S. Miyahara, Y. Miyoshi, K. Kawano, and J. Ninomiya (2002), Seasonal variation of non-migrating semidiurnal tide in the polar MLT region in a general circulation model, *J. Atmos. Terr. Phys.*, 64, 1083–1094.

Yee, J.-H., G. E. Cameron, and D. Y. Kusnierkiewicz (1999), Overview of TIMED, *Proc. SPIE*, 3756, 244–254.

Zhang, X., J. M. Forbes, M. E. Hagan, J. M. Russell, S. E. Palo, C. J. Mertens, and M. G. Mlynczak (2006), Monthly tidal temperatures 20–120 km from TIMED/SABER, *J. Geophys. Res.*, 111, A10S08, doi:10.1029/2005JA011504.

D. C. Fritts and H. Iimura, Colorado Research Associates Division, NorthWest Research Associates Inc., Boulder, CO 80301, USA. (iimurah@cora.nwra.com)

S. E. Palo, Department of Aerospace Engineering Sciences, University of Colorado at Boulder, Boulder, CO 80309, USA.

W. R. Skinner, Space Physics Research Laboratory, University of Michigan, Ann Arbor, MI 48109, USA.

Q. Wu, High Latitude Observatory, National Center for Atmospheric Research, Boulder, CO 80307, USA.